THE JOURNAL OF PHYSICAL CHEMISTRY Letters

pubs.acs.org/JPCL Letter

# Intramolecular Band Alignment and Spin−Orbit Coupling in Two-Dimensional Halide Perovskites

Linghai Zhang, Xu Zhang, and Gang Lu*

Cite This: J. Phys. Chem. Lett. 2020, 11, 6982−6989 Read Online

ACCESS | Metrics & More | Article Recommendations | Supporting Information

**ABSTRACT:** In two-dimensional (2D) halide perovskites, four distinct types of intramolecular band alignment ($I_a$, $I_b$, $II_a$, and $II_b$) can be formed between the organic and inorganic components. Molecular design to achieve desirable band alignments is of crucial importance to the applications of 2D perovskites and their heterostructures. In this work, by means of first-principles calculations, we have developed molecular design strategies that lead to the discovery of 2D halide perovskites with favorable band alignments toward light-emitting and photovoltaic applications. The same design strategies can be extended to vertical and lateral heterostructures of 2D perovskites with selective light emissions from the organic and/or inorganic layer of constituent 2D perovskites. For each intramolecular band alignment, the charge density and binding energy of the lowest energy exciton are examined. The effect of spin−orbit coupling (SOC) on the band structures is assessed. While SOC significantly lowers the band gaps in type-$I_a$ and type-$II_a$ alignments, it has a negligible effect in type-$I_b$ and type-$II_b$ alignments.

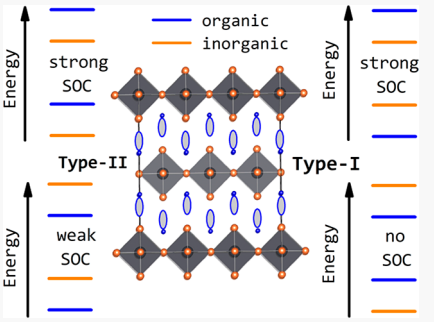


Hybrid organic−inorganic halide perovskites have emerged as highly promising optoelectronic materials with applications in light-emitting diodes (LEDs), photovoltaics, lasers, and photodetectors, etc.[1−4] However, three-dimensional (3D) halide perovskites are not stable and tend to degrade in the presence of light, heat, and humid air,[5−12] which severely hampers their applications. To overcome this critical problem, significant recent attention has been paid to their two-dimensional (2D) counterparts, which have demonstrated much improved stability and water resistance.[13−16] The 2D halide perovskites comprise inorganic metal−halide layers separated by organic spacers, and thus can be considered as quantum wells with the inorganic layers acting as "wells" and the organic spacers as "barriers". The chemical composition and thickness of the inorganic and organic layers can be tuned independently to offer much broader structural versatility and optoelectronic tunability than 3D perovskites.[17−21] Indeed, some of the most appealing characteristics of 2D perovskites stem from the tunability of their organic and inorganic components.[22−26]

Band alignment is the most fundamental feature underlying the optoelectronic applications of 2D perovskites. On the basis of the lowest unoccupied molecular orbital (LUMO) and the highest occupied molecular orbital (HOMO) of the organic and inorganic components, four types of intramolecular band alignment (two of type-I and two of type-II) can be formed in 2D perovskites, shown schematically in Figure 1a. The type-I band alignment is usually associated with lasers and LED applications, whereas the type-II alignment is necessary for photovoltaic applications.[27] The presence of two distinct type-I alignments ($I_a$ and $I_b$) enables selective light emission from either the organic or inorganic layer. While the former is often associated with $\pi^*-\pi$ transitions in organic chromophores, the latter can be characterized as interband transitions in quantum dots.[28−30] More importantly, design strategies in tuning their properties could vary significantly. For example, the exciton binding energy of the inorganic component can be tuned by 1−2 orders of magnitude by altering the thickness of the inorganic layer.[31] However, the same approach would have much less impact on the organic component. The presence of two distinct type-II alignments allows charge carriers to be separated in different layers, e.g., electrons in the inorganic layer and holes in the organic layer for $II_a$ alignment and vice versa for $II_b$ alignment. Since charge carriers are much more mobile in the inorganic layer than in the organic layer, the two band alignments could yield drastically different device performances. In some special cases, the band offset in the organic or inorganic layer could vanish, forming so-called type-V or VI band alignment defined in ref 32.[32]

Intramolecular band alignment also plays a crucial role in the optoelectronic properties of 2D perovskite heterostructures. While vertical heterostructures can be readily formed (or even unavoidable) in 2D perovskites,[33−36] lateral heterostructures were realized only recently.[37] For a heterostructure, one can

Received: July 14, 2020
Accepted: August 5, 2020
Published: August 5, 2020

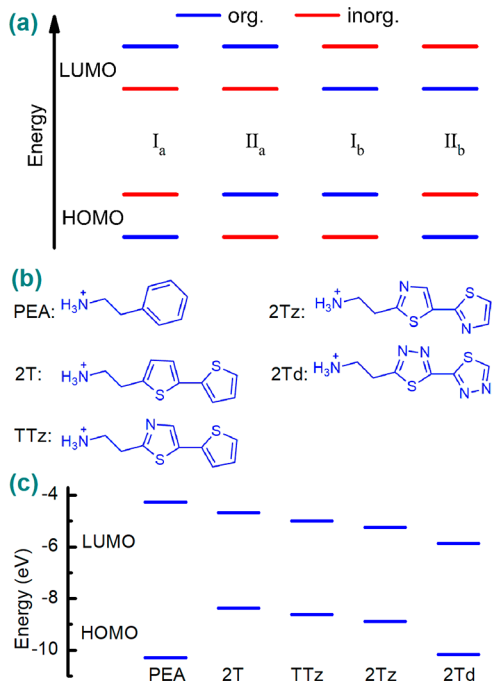


**Figure 1.** (a) Schematic illustration of four possible intramolecular band alignments ($I_a$, $II_a$, $I_b$, and $II_b$). The frontier energy levels belonging to the organic and inorganic component are shown in blue and red, respectively. (b) Chemical structures of PEA, 2T, TTz, 2Tz, and 2Td organic cations. (c) HOMO and LUMO levels of PEA, 2T, TTz, 2Tz, and 2Td cations using HSE/6-31G*.

infer its intermolecular band alignment from intramolecular band alignments of constituent perovskites, except perhaps near the heterojunction. For example, both $(2T)_2SnI_4$ and $(2T)_2PbI_4$ have type-I band alignment [2T = $(C_4H_3S)$-$(C_4H_2S)CH_2CH_2NH_3^+$], and thus, their lateral heterostructure $(2T)_2SnI_4$-$(2T)_2PbI_4$ was found to exhibit two distinct photoluminescence peaks, one from each component. Similarly, $(2T)_2PbI_4$ and $(2T)_2PbBr_4$ are of type-I and type-II alignment, respectively, and as a result, photoluminescence was detected only in $(2T)_2PbI_4$ of the lateral heterostructure.[37] Hence, one can engineer the band structure of a 2D perovskite heterostructure by tuning the intramolecular band alignments of constituent 2D perovskites.

Indeed, a number of first-principles studies have been performed to examine how optoelectronic properties may be modified by molecular tuning of 2D perovskites. For example, Quarti et al. showed that the optoelectronic properties can be regulated by the alkyl chain spacers of 2D perovskites.[38] Liu et al. revealed that the intramolecular band alignment of 2D perovskites can be tuned by the length of $\pi$-conjugated groups in spacer cations.[19] In our previous work, we have demonstrated that thermal fluctuations at room temperature could lead to variable intermolecular band alignments in 2D perovskite heterostructures.[36] Despite valuable insights offered by the previous works, there is no systematic study on the design strategies to yield desirable intramolecular band alignments in 2D perovskites, and our work aims to fill this gap.

It is known that spin−orbit coupling (SOC) is strong in halide perovskites containing heavy elements. And many first-principles calculations have been carried out to elucidate the SOC effect on the band structures of lead halide perovskites.[39−41] While a strong SOC effect has been found in 2D perovskites with alkyl chain spacers, such as $(C_4H_9NH_3)_2PbI_4$ and with short conjugated organic spacers, such as (pF $C_6H_5C_2H_4NH_3)_2PbI_4$, it remains to be seen whether a strong SOC effect could manifest in 2D perovskites with long conjugated organic spacers (e.g., 2T cations). In this case, the frontier orbitals may originate from the organic layers with negligible SOC effect. Herein, we carry out first-principles calculations, paying particular attention to SOC, to explore design strategies for desired intramolecular band alignments, which pave the way for rational design of 2D perovskites for novel optoelectronic applications.

In this work, we start with two prototypical 2D lead halide perovskites, $(PEA)_2PbI_4$ (PEA = $C_6H_5(CH_2)_2NH_3^+$) and $(2T)_2PbI_4$, whose molecular structures were obtained from experiments.[18,42] All ground state properties of the 2D perovskites were determined based on density functional theory (DFT) as implemented in Vienna Ab initio Simulation Package.[43] The Perdew−Burke−Ernzerhof functional[44] with an energy cutoff of 400 eV was employed to determine optimized molecular structures of the perovskites with the force convergence criterion set at 0.01 eV/Å. The pseudopotentials of the ionic cores were described by the projector augmented wave method[45] and Grimme's DFT-D2 correction was used to capture van der Waals interaction.[46] The Brillouin zone was sampled by a 4 × 4 × 1 Monkhorst−Pack grid for $(PEA)_2PbI_4$, and a 2 × 2 × 1 grid for other 2D perovskites. The calculated lattice parameters of $(PEA)_2PbI_4$ and $(2T)_2PbI_4$ agree well with the experimental values (Table S1 in Supporting Information).[18,42] For band structure calculations, Heyd−Scuseria−Ernzerhof (HSE) hybrid functional[47] with 43% of Hartree−Fock exchange was adopted in conjunction with a 5 × 5 × 1 and 3 × 3 × 1 Monkhorst−Pack grid for $(PEA)_2PbI_4$ and the other perovskites, respectively. Linear-response time-dependent density functional theory (LT-TDDFT)[48] with optimally tuned, screened and range-separated hybrid exchange−correlation functionals (OT-SRSH)[49−51] was employed to obtain the excitonic properties of the 2D perovskites.[52−54] In particular, the exciton binding energy is calculated as the difference between the fundamental gap and the optical gap determined from the LR-TDDFT-OT-SRSH calculations. A brief introduction to the LR-TDDFT-OT-SRSH method is shown in the Supporting Information. For LR-TDDFT-OT-SRSH calculations, a 2 × 2 × 1 supercell was used for $(PEA)_2PbI_4$ and a $\sqrt{2} \times \sqrt{2} \times 1$ supercell was used for the other perovskites. Due to the large supercells in the LR-TDDFT-OT-SRSH calculations, only the Γ-point in the Brillouin zone was sampled. We have also determined optimized molecular structures and HOMO/LUMO levels of isolated organic spacer cations using Gaussian 09 package[55] with the HSE functional (HSEH1PBE) and 6-31G* basis set.

First, we discuss design strategies to achieve type-$I_a$ band alignment. To simplify the discussion, we start with $PbI_4^{2-}$ as the inorganic component of 2D perovskites. To form type-$I_a$ alignment, the organic component needs to have a larger LUMO−HOMO gap than the inorganic component $PbI_4^{2-}$. Thus, we consider five organic cations (PEA, 2T, TTz, 2Tz, and 2Td) with relatively large HOMO−LUMO gaps. As shown in Figure 1b, each organic cation comprises a conjugated moiety, including benzene, thiophene, thiazole, and thiadiazole. Among them, thiazole and thiadiazole are strong electron withdrawn moieties, and the organic cations


https://dx.doi.org/10.1021/acs.jpclett.0c02135
J. Phys. Chem. Lett. 2020, 11, 6982−6989

containing them are expected to have lower LUMO levels, as shown in Figure 1c.

Five 2D perovskites with chemical formula of $(PEA)_2PbI_4$, $(2T)_2PbI_4$, $(TTz)_2PbI_4$, $(2Tz)_2PbI_4$, and $(2Td)_2PbI_4$ are designed by combining the five organic cations with the inorganic $PbI_4^{2-}$ layer (their optimized molecular structures are shown in Figure S1). The band alignments of the 2D perovskites are displayed in Figure 2a. In the presence of SOC,

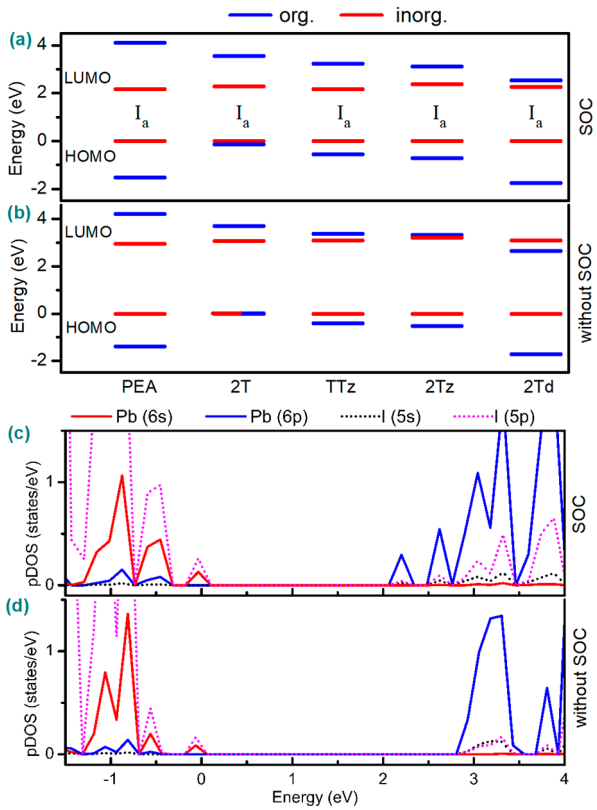


**Figure 2.** Band alignment of $(PEA)_2PbI_4$, $(2T)_2PbI_4$, $(TTz)_2PbI_4$, $(2Tz)_2PbI_4$, and $(2Td)_2PbI_4$ 2D perovskites using HSE+SOC (a) and HSE without SOC (b). Projected density of states of $(PEA)_2PbI_4$ 2D perovskite calculated using HSE+SOC (c) and HSE without SOC (d). The HOMO level of the inorganic layer is set to zero.

all perovskites are predicted to exhibit type-$I_a$ band alignment, with the band gap of the inorganic component smaller than that of the organic component. With type-$I_a$ band alignment, the lowest energy exciton is predicted to reside in the inorganic layer, while higher energy excitons are expected to relax and transfer quickly to the inorganic layer, from which light emission takes place. Similar to experimental estimates (0.2–0.3 eV),[56] the exciton binding energy is found to be quite high (~0.35 eV), which enables a strong photoluminescence from $PbI_4^{2-}$ layer. In Figure 3a, we present the charge density of the lowest energy exciton in $(PEA)_2PbI_4$ with the electron and hole density colored in yellow and cyan, respectively. Although localized in the out-of-plane direction, the exciton is delocalized within the inorganic layer, resembling Wannier excitons in solids.[57]

As shown in Figure 2a, tuning the organic layer from PEA to 2T, TTz, 2Tz, and 2Td lowers the energy offset between unoccupied levels, and for $(2T)_2PbI_4$, also the energy offset between occupied levels. These could have some undesirable consequences: (1) There could be resonant tunneling for

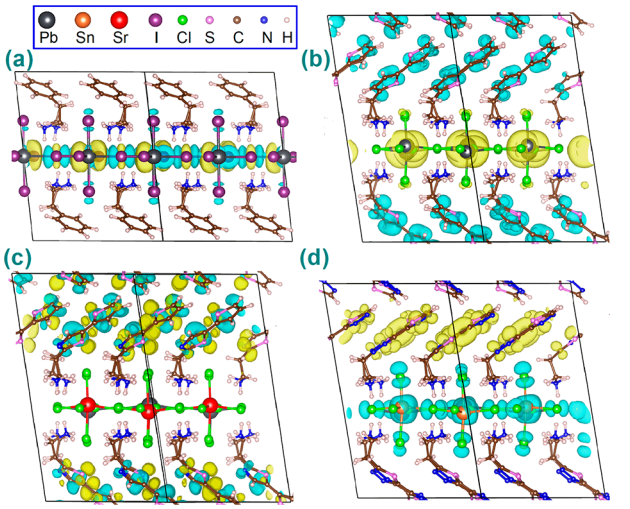


**Figure 3.** Charge density of the lowest-energy exciton in (a) $(PEA)_2PbI_4$, (b) $(2T)_2PbCl_4$, (c) $(TTz)_2Pb_{0.5}Sr_{0.5}Cl_4$, and (d)-$(2Td)_2Pb_{0.5}Sn_{0.5}Cl_4$. The electron and hole densities are colored in yellow and cyan, respectively.

electrons in $(2Td)_2PbI_4$ and holes in $(2T)_2PbI_4$ between the organic and inorganic layers. (2) Thermal fluctuations at room temperature may lead to oscillatory band alignment between type $I_a$ and type $II_a$ in $(2T)_2PbI_4$, owing to the "softness" of the inorganic layers.[58] Hence, among the five perovskites, $(PEA)_2PbI_4$, $(TTz)_2PbI_4$, and $(2Tz)_2PbI_4$ possess more favorable band alignment for LED applications, particularly the last two with lower energy offsets.

The SOC is shown to have a strong effect on the band structures of the 2D perovskites (see Figure 2a,b). In particular, the conduction band minimums (CBMs) are lowered by ~0.7 eV, while the valence band maximums (VBMs) remain largely unchanged (~0.1 eV). As a result, the band gaps are reduced by ~0.8 eV. For example, the band gap of $(PEA)_2PbI_4$ calculated by HSE+SOC is 2.17 eV, consistent with previous experiments (2.28–2.35 eV),[59] while the band gap calculated by HSE without SOC correction is 2.97 eV. We can understand these results from the projected density of states (pDOS) shown in Figure 2c,d. The CBM is originated from Pb 6p orbitals while the VBM is dominated by I 5p orbitals. Since SOC is stronger in the heavier element Pb than I, the shift in CBM is much larger than that in VBM.

Panels a and b of Figure 4 display the band structures of $(PEA)_2PbI_4$ obtained from HSE+SOC and HSE calculations, respectively. A direct band gap at Γ point is observed and there is strong dispersion of the CBM and VBM bands along X–Γ–Y directions, yielding small effective masses for charge carriers in the inorganic layer (see Table 1). In contrast, there is negligible dispersion for the bands along Γ–M (out-of-plane) direction, giving rise to much lower carrier mobilities normal to the inorganic layer.

Next, we discuss design strategies to achieve type-$II_a$ band alignment in 2D perovskites. The type-$II_a$ alignment requires that the HOMO of the organic component be higher than that of the inorganic component. To meet this requirement, we select 2T as the organic component, which has a high HOMO level owing to its electron donating moiety (thiophene). At the same time, we need to lower the HOMO level (or increase the band gap) of the inorganic component. It is known that replacing I by Cl in lead halide perovskites could increase their


https://dx.doi.org/10.1021/acs.jpclett.0c02135
J. Phys. Chem. Lett. 2020, 11, 6982–6989

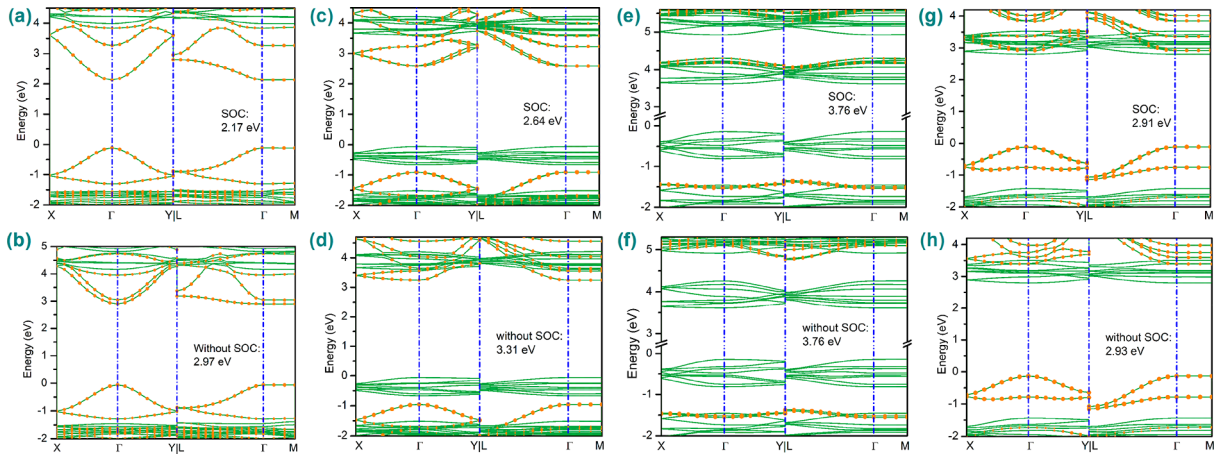


**Figure 4.** Band structure of (a) $(PEA)_2PbI_4$, (c) $(2T)_2PbCl_4$, (e) $(TTz)_2Pb_{0.5}Sr_{0.5}Cl_4$, and (g)$(2Td)_2Pb_{0.5}Sn_{0.5}Cl_4$ using HSE+SOC. Band structure of (b) $(PEA)_2PbI_4$, (d) $(2T)_2PbCl_4$, (f) $(TTz)_2Pb_{0.5}Sr_{0.5}Cl_4$, and (h) $(2Td)_2Pb_{0.5}Sn_{0.5}Cl_4$ using HSE without SOC. The Femi level is set to zero. The high-symmetry points are labeled by Γ (0, 0, 0), X (0.5, 0, 0), Y (0, 0.5, 0), L (0.5, 0.5, 0), and M (0, 0, 0.5). The band gap values are also shown in the figure. The band contributions due to the inorganic and organic component are shown with green curves with and without orange dots, respectively.

**Table 1. Effective Masses (Using HSE+SOC) Obtained by Parabolic Fitting to Figure 4 for CBM and VBM along Γ−X and Γ−Y Directions for the 2D Perovskites**

| | $(PEA)_2PbI_4$ | | $(2T)_2PbCl_4$ | | $(TTz)_2Pb_{0.5}Sr_{0.5}Cl_4$ | | $(2Td)_2Pb_{0.5}Sn_{0.5}Cl_4$ | |
|---|---|---|---|---|---|---|---|---|
| | CBM | VBM | CBM | VBM | CBM | VBM | CBM | VBM |
| Γ−X | 0.26 | 0.30 | 0.56 | 1.23 | 9.12 | 1.15 | 3.40 | 0.35 |
| Γ−Y | 0.25 | 0.30 | 0.30 | 6.25 | 2.57 | 8.59 | 2.41 | 0.35 |

band gaps; we thus consider $PbCl_4^{2-}$, $Pb_{0.5}Sn_{0.5}Cl_4^{2-}$, and $Pb_{0.5}Sr_{0.5}Cl_4^{2-}$ as the inorganic component to form three 2D perovskites, $(2T)_2PbCl_4$, $(2T)_2Pb_{0.5}Sn_{0.5}Cl_4$, and $(2T)_2Pb_{0.5}Sr_{0.5}Cl_4$.

As shown in Figure 5a, the band gap of the inorganic layer $PbI_4^{2-}$, $Pb_{0.5}Sn_{0.5}Cl_4^{2-}$, $PbCl_4^{2-}$, and $Pb_{0.5}Sr_{0.5}Cl_4^{2-}$ is calculated as 2.28, 3.08, 3.50, and 5.28 eV, respectively. As a result, a robust type-$II_a$ band alignment is predicted to form in $(2T)_2PbCl_4$ and $(2T)_2Pb_{0.5}Sn_{0.5}Cl_4$, which is necessary for photovoltaic applications. However, $(2T)_2Pb_{0.5}Sr_{0.5}Cl_4$ is not a good candidate because of its very small conduction band offset. In Figure 3b, we present the charge density of the lowest energy exciton in $(2T)_2PbCl_4$ with the electron and hole density shown in yellow and cyan, respectively. The exciton exhibits a strong charge-transfer character, with electron confined in the inorganic layer and hole in the organic layer. Although the exciton binding energy is high (~0.30 eV), one can lower it by increasing the thickness of the inorganic layers. The strategy to lower the exciton binding energy while maintain $II_a$ band alignment is an open question and needs to be addressed in the future. The band structure shown in Figure 4c and the effective masses in Table 1 suggest that the electrons in $PbCl_4^{2-}$ layer have much higher in-plane mobilities than the holes in 2T layer. Once again, SOC significantly lowers the CBM of the inorganic layers (see Figure 5a and 5b). In particular, it lowers the CBM and band gap of $(2T)_2PbCl_4$ by more than 0.6 eV.

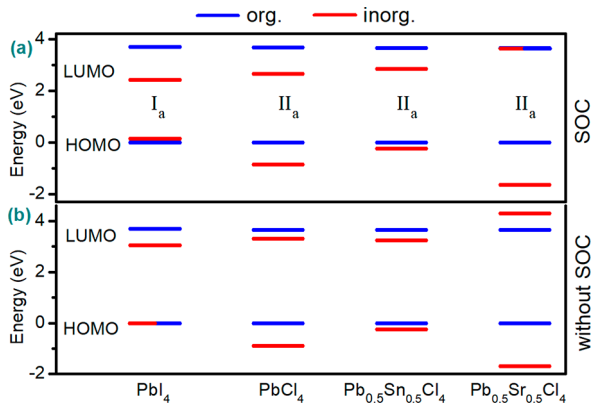


**Figure 5.** (a) Band alignment of $(2T)_2PbI_4$, $(2T)_2PbCl_4$, $(2T)_2Pb_{0.5}Sn_{0.5}Cl_4$, and $(2T)_2Pb_{0.5}Sr_{0.5}Cl_4$ using HSE+SOC (a) and HSE without SOC (b). The HOMO of the organic layer is set to zero. The LUMO of $Pb_{0.5}Sr_{0.5}Cl_4^{2-}$ is slightly lower than that of the organic layer with 2T cations in Figure 5a. The optimized structures of these 2D perovskites are shown in Figure S2.

We then discuss the strategy to form type-$I_b$ band alignment in 2D perovskites, which requires the band gap of the inorganic component be larger than that of the organic component. To this end, we turn to $Pb_{0.5}Sr_{0.5}Cl_4^{2-}$ as the inorganic layer because it has a wide band gap (5.28 eV) as discussed above. As shown in Figure 5a, the conduction band offset of $(2T)_2Pb_{0.5}Sr_{0.5}Cl_4$ is quite small. Thus, if the LUMO level of the organic layer in $(2T)_2Pb_{0.5}Sr_{0.5}Cl_4$ can be lowered, we could achieve type-$I_b$ alignment. As indicated in Figure 1c, TTz, 2Tz, and 2Td cations have a lower LUMO level than 2T. Hence, we can combine TTz, 2Tz, and 2Td with $Pb_{0.5}Sr_{0.5}Cl_4^{2-}$ to form type-$I_b$ band alignment.

As shown in Figure 6a, this strategy is successful and type-$I_b$ band alignment is achieved in $(TTz)_2Pb_{0.5}Sr_{0.5}Cl_4$, $(2Tz)_2Pb_{0.5}Sr_{0.5}Cl_4$, and $(2Td)_2Pb_{0.5}Sr_{0.5}Cl_4$ 2D perovskites, with the first two being more robust than the last. In these perovskites, the lowest (singlet) exciton is predicted to be localized in the organic layer, shown in Figure 3c with $(TTz)_2Pb_{0.5}Sr_{0.5}Cl_4$ as an example. Although the triplet exciton is expected to have a lower energy than the singlet exciton,[60] the detailed study of triplet excitons is beyond the scope of the present paper. The singlet exciton is found to be Frenkel type with a binding energy of 0.32 eV, which likely leads to strong light emission from the organic layer.



https://dx.doi.org/10.1021/acs.jpclett.0c02135
J. Phys. Chem. Lett. 2020, 11, 6982−6989

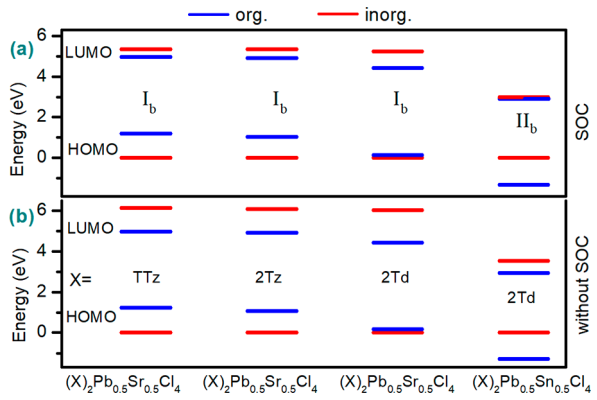


**Figure 6.** (a) Band alignment of $(TTz)_2Pb_{0.5}Sr_{0.5}Cl_4$, $(2Tz)_2Pb_{0.5}Sr_{0.5}Cl_4$, $(2Td)_2Pb_{0.5}Sr_{0.5}Cl_4$, and $(2Td)_2Pb_{0.5}Sn_{0.5}Cl_4$ using HSE+SOC (a) and HSE without SOC (b). The HOMO of the inorganic layer is set to zero. The LUMO of $Pb_{0.5}Sn_{0.5}Cl_4^{2-}$ is slightly higher than that of the organic layers with 2Td cations in Figure 6a. The optimized structures of the 2D perovskites are shown in Figure S3.

Interestingly, SOC has no effect on the band gaps of these 2D perovskites (see Figure 6a,b). This is because their band gaps are determined by the HOMO/LUMO levels of the organic layers, which are not affected by SOC. As shown in Figure 4e,f, the direct band gap at the Gamma point is 3.76 eV for $(TTz)_2Pb_{0.5}Sr_{0.5}Cl_4$, independent of SOC. However, the conduction band offset is reduced due to the SOC effect on the inorganic layer. The charge carriers are predicted to have large effective masses owing to the weak dispersion of the organic bands (see Table 1).

Finally, we explore the strategy to form type-$II_b$ band alignment in 2D perovskites. Type-$II_b$ band alignment is opposite to type-$II_a$, requiring HOMO and LUMO levels of the organic component be lowered. To meet this requirement, we turn to type-$II_a$ band alignment for a clue. We note in Figure 5a although $(2T)_2Pb_{0.5}Sn_{0.5}Cl_4$ has type-$II_a$ alignment, its valence band offset is small. If HOMO/LUMO levels of the organic component are lowered, we could switch the band alignment from $II_a$ to $II_b$. Since 2Td has the lowest LUMO and HOMO levels among the organic cations examined above, we propose to replace 2T by 2Td and combine it with $Pb_{0.5}Sn_{0.5}Cl_4^{2-}$ to form 2D perovskite $(2Td)_2Pb_{0.5}Sn_{0.5}Cl_4$.

The band alignment of $(2Td)_2Pb_{0.5}Sn_{0.5}Cl_4$ is shown in Figure 6a, which exhibits type-$II_b$ as hoped. However, its conduction band offset is too small, and its band alignment may oscillate between $I_a$ and $II_b$ driven by thermal fluctuations. The charge density of the lowest energy exciton is shown in Figure 3d with the electron and hole density in yellow and cyan, respectively. Although the exciton has a large binding energy of 0.31 eV, the photoexcited electron and hole are well separated at the organic and inorganic layer, respectively. The charge-transfer exciton is expected to have a longer lifetime. As shown in Figure 4g, there is a direct band gap at the Γ point, and the holes are predicted to have smaller effective masses than the electrons (see Table 1). We find that SOC has negligible influence on the band gap (2.91 eV) because it has no effect on the organic layer and negligible effect on the VBM of the inorganic layer. However, SOC can significantly reduce the conduction band offset.

Since various 2D perovskites have been designed for the four types of band alignment, we could in principle combine them to form vertical or lateral heterostructures with appropriate band alignments. We provide an initial effort to design a lateral heterostructure with a desired band alignment. Our effort is motivated by recent experiments that demonstrated photoluminescence emissions from two separate 2D perovskites within a lateral heterostructure.[37] Here, we predict a new lateral heterostructure consisting of 2D perovskites, $(2Tz)_2Pb_{0.5}Sn_{0.5}Cl_4$ and $(2Tz)_2Pb_{0.5}Sr_{0.5}Cl_4$. The two perovskites have similar lattice constants (see Table S1) with less than 1% of lattice mismatch. Moreover, Sn-doped 2D lead halide perovskites are known to host self-trapped excitons, which could generate broadband emission at room temperature with a high quantum yield.[61] The schematic illustration of the lateral heterostructure is shown in Figure 7a and the

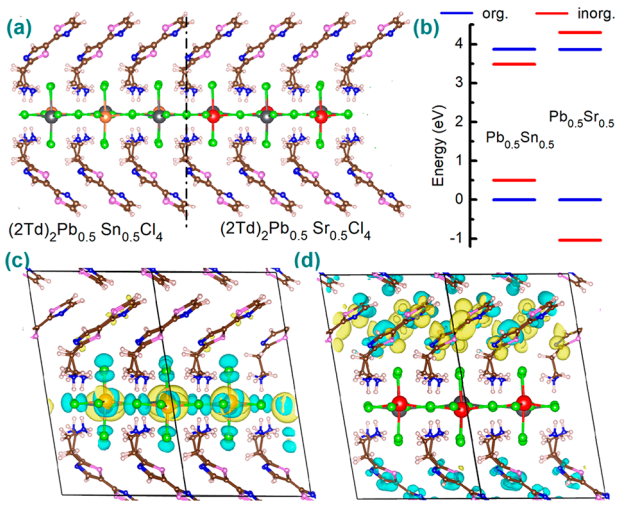


**Figure 7.** (a) Schematic illustration of $(2Tz)_2Pb_{0.5}Sn_{0.5}Cl_4$-$(2Tz)_2Pb_{0.5}Sr_{0.5}Cl_4$ lateral heterostructure. (b) Intermolecular band alignment of the lateral heterostructure calculated by HSE+SOC. The HOMO of the organic layers is set to zero. (c) Charge density of the lowest energy exciton in $(2Tz)_2Pb_{0.5}Sn_{0.5}Cl_4$. (d) Charge density of the lowest energy singlet exciton in $(2Tz)_2Pb_{0.5}Sr_{0.5}Cl_4$. The electron and hole densities are shown in yellow and cyan, respectively.

band alignment ($I_a$–$I_b$) of the lateral heterostructure is shown in Figure 7b, determined from HSE+SOC calculations. This lateral heterostructure is predicted to yield photoluminescence from the organic layer in $(2Tz)_2Pb_{0.5}Sr_{0.5}Cl_4$ and Sn-doped inorganic layer in $(2Tz)_2Pb_{0.5}Sn_{0.5}Cl_4$. The charge densities of the lowest energy excitons in $(2Tz)_2Pb_{0.5}Sn_{0.5}Cl_4$ and $(2Tz)_2Pb_{0.5}Sr_{0.5}Cl_4$ are shown in Figure 7c,d, respectively. The exciton in the inorganic layer is of delocalized Wannier type while the singlet exciton in the organic layer is of localized Frenkel type.[62,63]

To summarize, we have developed design strategies to achieve various band alignments in 2D perovskites based on first-principles calculations. Eight distinct 2D perovskites are predicted to exhibit either type-$I_a$ or type-$I_b$ band alignment, which enables light-emitting applications. Four different 2D perovskites are predicted to exhibit either type-$II_a$ or type-$II_b$ band alignment, which allows for photovoltaic applications. For type-$I_a$ and type-$I_b$ alignment, the lowest energy exciton is confined to the inorganic and organic layer, respectively. The lowest exciton is estimated to have a large binding energy (~0.35 eV), with resemblance of a Wannier exciton delocalized in the inorganic layer (for type-$I_a$) or a Frenkel exciton localized in the organic layer (for type-$I_b$). In contrast,


https://dx.doi.org/10.1021/acs.jpclett.0c02135
J. Phys. Chem. Lett. 2020, 11, 6982−6989

the type-$II_a$ (or type-$II_b$) band alignment hosts charge-transfer excitons with the electrons (holes) and holes (electrons) residing in the inorganic and organic layer, respectively. We demonstrate the possibility to design 2D perovskite heterostructures with appropriate band alignments based on intramolecular band alignments of constituent perovskites. The band structure for each type of band alignment is examined and corresponding effective masses for charge carriers along different directions are estimated. SOC is revealed to have a strong effect on the conduction bands of the inorganic layers; it can lower the band gaps in type-$I_a$ and type-$II_a$ alignments by 0.6−0.8 eV, but it has a negligible effect on type-$I_b$ and $II_b$ alignments. Therefore, to estimate the band gap in type-$I_b$ or type-$II_b$ alignment, one can ignore SOC in the HSE calculations. Finally, this work could provide valuable insight to the development of 2D perovskites for novel optoelectronic applications.

## ■ ASSOCIATED CONTENT

### Supporting Information

The Supporting Information is available free of charge at https://pubs.acs.org/doi/10.1021/acs.jpclett.0c02135.

Brief introduction of the LR-TDDFT-OT-SRSH method, the calculated lattice parameters of the designed 2D perovskites, the optimized structures of the designed 2D perovskites (PDF)

## ■ AUTHOR INFORMATION


### Corresponding Author

**Gang Lu** − *Department of Physics and Astronomy, California State University, Northridge, Northridge, California 91330-8268, United States;* orcid.org/0000-0002-9168-8968; Email: ganglu@csun.edu

### Authors

**Linghai Zhang** − *Department of Physics and Astronomy, California State University, Northridge, Northridge, California 91330-8268, United States;* orcid.org/0000-0003-0536-5765

**Xu Zhang** − *Department of Physics and Astronomy, California State University, Northridge, Northridge, California 91330-8268, United States;* orcid.org/0000-0002-6491-3234

Complete contact information is available at: https://pubs.acs.org/10.1021/acs.jpclett.0c02135


### Notes

The authors declare no competing financial interest.

## ■ ACKNOWLEDGMENTS

The work was supported by the U.S. National Science Foundation (DMR1828019) and the U.S. Army Research Office (W911NF1810473).

## ■ REFERENCES


(1) Tan, Z.-K.; Moghaddam, R. S.; Lai, M. L.; Docampo, P.; Higler, R.; Deschler, F.; Price, M.; Sadhanala, A.; Pazos, L. M.; Credgington, D.; et al. Bright Light-Emitting Diodes Based on Organometal Halide Perovskite. *Nat. Nanotechnol.* **2014**, *9*, 687−692.

(2) Dou, L.; Yang, Y.; You, J.; Hong, Z.; Chang, W.-H.; Li, G.; Yang, Y. Solution-Processed Hybrid Perovskite Photodetectors with High Detectivity. *Nat. Commun.* **2014**, *5*, 5404.

(3) Li, Y. J.; Lv, Y.; Zou, C.-L.; Zhang, W.; Yao, J.; Zhao, Y. S. Output Coupling of Perovskite Lasers from Embedded Nanoscale Plasmonic Waveguides. *J. Am. Chem. Soc.* **2016**, *138*, 2122−2125.

(4) Kong, X.; Jiang, Y.; Wu, X.; Chen, C.; Guo, J.; Liu, S.; Gao, X.; Zhou, G.; Liu, J.-M.; Kempa, K.; et al. Dopant-Free F-Substituted Benzodithiophene Copolymer Hole-Transporting Materials for Efficient and Stable Perovskite Solar Cells. *J. Mater. Chem. A* **2020**, *8*, 1858−1864.

(5) Niu, G.; Guo, X.; Wang, L. Review of Recent Progress in Chemical Stability of Perovskite Solar Cells. *J. Mater. Chem. A* **2015**, *3*, 8970−8980.

(6) Han, Y.; Meyer, S.; Dkhissi, Y.; Weber, K.; Pringle, J. M.; Bach, U.; Spiccia, L.; Cheng, Y.-B. Degradation Observations of Encapsulated Planar $CH_3NH_3PbI_3$ Perovskite Solar Cells at High Temperatures and Humidity. *J. Mater. Chem. A* **2015**, *3*, 8139−8147.

(7) He, J.; Fang, W.-H.; Long, R.; Prezhdo, O. V. Superoxide/Peroxide Chemistry Extends Charge Carriers' Lifetime but Undermines Chemical Stability of $CH_3NH_3PbI_3$ Exposed to Oxygen: Time-Domain ab Initio Analysis. *J. Am. Chem. Soc.* **2019**, *141*, 5798−5807.

(8) Tong, C.-J.; Geng, W.; Tang, Z.-K.; Yam, C.-Y.; Fan, X.-L.; Liu, J.; Lau, W.-M.; Liu, L.-M. Uncovering the Veil of the Degradation in Perovskite $CH_3NH_3PbI_3$ upon Humidity Exposure: A First-Principles Study. *J. Phys. Chem. Lett.* **2015**, *6*, 3289−3295.

(9) Sun, P.-P.; Chi, W.-J.; Li, Z.-S. Effects of Water Molecules on the Chemical Stability of $MAGeI_3$ Perovskite Explored from A Theoretical Viewpoint. *Phys. Chem. Chem. Phys.* **2016**, *18*, 24526−24536.

(10) Nan, G.; Zhang, X.; Lu, G. Self-Healing of Photocurrent Degradation in Perovskite Solar Cells: The Role of Defect-Trapped Excitons. *J. Phys. Chem. Lett.* **2019**, *10*, 7774−7780.

(11) Zhang, L.; Sit, P. H. L. Ab Initio Study of the Dynamics of Electron Trapping and Detrapping Processes in the $CH_3NH_3PbI_3$ Perovskite. *J. Mater. Chem. A* **2019**, *7*, 2135−2147.

(12) Mosconi, E.; Azpiroz, J. M.; De Angelis, F. Ab Initio Molecular Dynamics Simulations of Methylammonium Lead Iodide Perovskite Degradation by Water. *Chem. Mater.* **2015**, *27*, 4885−4892.

(13) Grancini, G.; Roldán-Carmona, C.; Zimmermann, I.; Mosconi, E.; Lee, X.; Martineau, D.; Narbey, S.; Oswald, F.; De Angelis, F.; Graetzel, M.; et al. One-Year Stable Perovskite Solar Cells by 2D/3D Interface Engineering. *Nat. Commun.* **2017**, *8*, 15684.

(14) Stoumpos, C. C.; Cao, D. H.; Clark, D. J.; Young, J.; Rondinelli, J. M.; Jang, J. I.; Hupp, J. T.; Kanatzidis, M. G. Ruddlesden-Popper Hybrid Lead Iodide Perovskite 2D Homologous Semiconductors. *Chem. Mater.* **2016**, *28*, 2852−2867.

(15) Liu, G.; Zheng, H.; Xu, X.; Zhu, L.-Z.; Zhang, X.; Pan, X. Design of High-Efficiency and Environmentally Stable Mixed-Dimensional Perovskite Solar Cells Based on Cesium-Formamidinium Lead Halide Component. *Chem. Mater.* **2018**, *30*, 7691−7698.

(16) Yang, Y.; Gao, F.; Gao, S.; Wei, S.-H. Origin of the Stability of Two-Dimensional Perovskites: A First-Principles Study. *J. Mater. Chem. A* **2018**, *6*, 14949−14955.

(17) Mao, L.; Ke, W.; Pedesseau, L.; Wu, Y.; Katan, C.; Even, J.; Wasielewski, M. R.; Stoumpos, C. C.; Kanatzidis, M. G. Hybrid Dion-Jacobson 2D Lead Iodide Perovskites. *J. Am. Chem. Soc.* **2018**, *140*, 3775−3783.

(18) Gao, Y.; Shi, E.; Deng, S.; Shiring, S. B.; Snaider, J. M.; Liang, C.; Yuan, B.; Song, R.; Janke, S. M.; Liebman-Peláez, A.; et al. Molecular Engineering of Organic-Inorganic Hybrid Perovskites Quantum Wells. *Nat. Chem.* **2019**, *11*, 1151−1157.

(19) Liu, C.; Huhn, W.; Du, K.-Z.; Vazquez-Mayagoitia, A.; Dirkes, D.; You, W.; Kanai, Y.; Mitzi, D. B.; Blum, V. Tunable Semiconductors: Control over Carrier States and Excitations in Layered Hybrid Organic-Inorganic Perovskites. *Phys. Rev. Lett.* **2018**, *121*, 146401.

(20) Ju, M.-G.; Dai, J.; Ma, L.; Zhou, Y.; Liang, W.; Zeng, X. C. Lead-Free Low-Dimensional Tin Halide Perovskites with Functional Organic Spacers: Breaking the Charge-Transport Bottleneck. *J. Mater. Chem. A* **2019**, *7*, 16742−16747.

(21) Leng, K.; Abdelwahab, I.; Verzhbitskiy, I.; Telychko, M.; Chu, L.; Fu, W.; Chi, X.; Guo, N.; Chen, Z.; Chen, Z.; et al. Molecularly Thin Two-Dimensional Hybrid Perovskites with Tunable Optoelectronic Properties due to Reversible Surface Relaxation. *Nat. Mater.* **2018**, *17*, 908−914.
(22) Lai, H.; Kan, B.; Liu, T.; Zheng, N.; Xie, Z.; Zhou, T.; Wan, X.; Zhang, X.; Liu, Y.; Chen, Y. Two-Dimensional Ruddlesden-Popper Perovskite with Nanorod-like Morphology for Solar Cells with Efficiency Exceeding 15%. *J. Am. Chem. Soc.* **2018**, *140*, 11639−11646.
(23) Passarelli, J. V.; Fairfield, D. J.; Sather, N. A.; Hendricks, M. P.; Sai, H.; Stern, C. L.; Stupp, S. I. Enhanced Out-of-Plane Conductivity and Photovoltaic Performance in n = 1 Layered Perovskites through Organic Cation Design. *J. Am. Chem. Soc.* **2018**, *140*, 7313−7323.
(24) Liu, X.-K.; Gao, F. Organic-Inorganic Hybrid Ruddlesden-Popper Perovskites: An Emerging Paradigm for High-Performance Light-Emitting Diodes. *J. Phys. Chem. Lett.* **2018**, *9*, 2251−2258.
(25) Chao, L.; Niu, T.; Xia, Y.; Ran, X.; Chen, Y.; Huang, W. Efficient and Stable Low-Dimensional Ruddlesden-Popper Perovskite Solar Cells Enabled by Reducing Tunnel Barrier. *J. Phys. Chem. Lett.* **2019**, *10*, 1173−1179.
(26) Yang, X.; Zhang, X.; Deng, J.; Chu, Z.; Jiang, Q.; Meng, J.; Wang, P.; Zhang, L.; Yin, Z.; You, J. Efficient Green Light-Emitting Diodes Based on Quasi-Two-Dimensional Composition and Phase Engineered Perovskite with Surface Passivation. *Nat. Commun.* **2018**, *9*, 570.
(27) Wei, K.; Jiang, T.; Xu, Z.; Zhou, J.; You, J.; Tang, Y.; Li, H.; Chen, R.; Zheng, X.; Wang, S.; et al. Ultrafast Carrier Transfer Promoted by Interlayer Coulomb Coupling in 2D/3D Perovskite Heterostructures. *Laser Photonics Rev.* **2018**, *12*, 1800128.
(28) Chondroudis, K.; Mitzi, D. B. Electroluminescence from an Organic-Inorganic Perovskite Incorporating a Quaterthiophene Dye within Lead Halide Perovskite Layers. *Chem. Mater.* **1999**, *11*, 3028−3030.
(29) Liang, D.; Peng, Y.; Fu, Y.; Shearer, M. J.; Zhang, J.; Zhai, J.; Zhang, Y.; Hamers, R. J.; Andrew, T. L.; Jin, S. Color-Pure Violet-Light-Emitting Diodes Based on Layered Lead Halide Perovskite Nanoplates. *ACS Nano* **2016**, *10*, 6897−6904.
(30) Yin, J.; Li, H.; Cortecchia, D.; Soci, C.; Brédas, J.-L. Excitonic and Polaronic Properties of 2D Hybrid Organic-Inorganic Perovskites. *ACS Energy Lett.* **2017**, *2*, 417−423.
(31) Blancon, J. C.; Stier, A. V.; Tsai, H.; Nie, W.; Stoumpos, C. C.; Traoré, B.; Pedesseau, L.; Kepenekian, M.; Katsutani, F.; Noe, G. T.; et al. Scaling Law for Excitons in 2D Perovskite Quantum Wells. *Nat. Commun.* **2018**, *9*, 2254.
(32) Si, Y.; Wu, H.-Y.; Lian, J.-C.; Huang, W.-Q.; Hu, W.-Y.; Huang, G.-F. A Design Rule for Two-Dimensional Van der Waals Heterostructures with Unconventional Band Alignments. *Phys. Chem. Chem. Phys.* **2020**, *22*, 3037−3047.
(33) Qing, J.; Liu, X.-K.; Li, M.; Liu, F.; Yuan, Z.; Tiukalova, E.; Yan, Z.; Duchamp, M.; Chen, S.; Wang, Y.; et al. Aligned and Graded Type-II Ruddlesden-Popper Perovskite Films for Efficient Solar Cells. *Adv. Energy Mater.* **2018**, *8*, 1800185.
(34) Liu, J.; Leng, J.; Wu, K.; Zhang, J.; Jin, S. Observation of Internal Photoinduced Electron and Hole Separation in Hybrid Two-Dimentional Perovskite Films. *J. Am. Chem. Soc.* **2017**, *139*, 1432−1435.
(35) Wang, N.; Cheng, L.; Ge, R.; Zhang, S.; Miao, Y.; Zou, W.; Yi, C.; Sun, Y.; Cao, Y.; Yang, R.; et al. Perovskite Light-Emitting Diodes Based on Solution-Processed Self-organized Multiple Quantum Wells. *Nat. Photonics* **2016**, *10*, 699−704.
(36) Zhang, L.; Zhang, X.; Lu, G. Band Alignment in Two-Dimensional Halide Perovskite Heterostructures: Type I or Type II? *J. Phys. Chem. Lett.* **2020**, *11*, 2910−2916.
(37) Shi, E.; Yuan, B.; Shiring, S. B.; Gao, Y.; Akriti; Guo, Y.; Su, C.; Lai, M.; Yang, P.; Kong, J.; et al. Two-Dimensional Halide Perovskite Lateral Epitaxial Heterostructures. *Nature* **2020**, *580*, 614−620.
(38) Quarti, C.; Marchal, N.; Beljonne, D. Tuning the Optoelectronic Properties of Two-Dimensional Hybrid Perovskite Semiconductors with Alkyl Chain Spacers. *J. Phys. Chem. Lett.* **2018**, *9*, 3416−3424.
(39) Even, J.; Pedesseau, L.; Jancu, J.-M.; Katan, C. Importance of Spin-Orbit Coupling in Hybrid Organic/Inorganic Perovskites for Photovoltaic Applications. *J. Phys. Chem. Lett.* **2013**, *4*, 2999−3005.
(40) Wang, D.; Wen, B.; Zhu, Y.-N.; Tong, C.-J.; Tang, Z.-K.; Liu, L.-M. First-Principles Study of Novel Two-Dimensional $(C_4H_9NH_3)_2PbX_4$ Perovskites for Solar Cell Absorbers. *J. Phys. Chem. Lett.* **2017**, *8*, 876−883.
(41) Even, J.; Pedesseau, L.; Dupertuis, M. A.; Jancu, J. M.; Katan, C. Electronic Model for Self-Assembled Hybrid Organic/Perovskite Semiconductors: Reverse Band Edge Electronic States Ordering and Spin-Orbit Coupling. *Phys. Rev. B: Condens. Matter Mater. Phys.* **2012**, *86*, 205301.
(42) Ma, D.; Fu, Y.; Dang, L.; Zhai, J.; Guzei, I. A.; Jin, S. Single-Crystal Microplates of Two-Dimensional Organic-Inorganic Lead Halide Layered Perovskites for Optoelectronics. *Nano Res.* **2017**, *10*, 2117−2129.
(43) Kresse, G.; Furthmüller, J. Efficient Iterative Schemes for Ab Initio Total-Energy Calculations Using a Plane-Wave Basis Set. *Phys. Rev. B: Condens. Matter Mater. Phys.* **1996**, *54*, 11169−11186.
(44) Perdew, J. P.; Burke, K.; Ernzerhof, M. Generalized Gradient Approximation Made Simple. *Phys. Rev. Lett.* **1996**, *77*, 3865−3868.
(45) Blöchl, P. E. Projector Augmented-Wave Method. *Phys. Rev. B: Condens. Matter Mater. Phys.* **1994**, *50*, 17953−17979.
(46) Grimme, S. Semiempirical GGA-Type Density Functional Constructed with A Long-Range Dispersion Correction. *J. Comput. Chem.* **2006**, *27*, 1787−1799.
(47) Heyd, J.; Scuseria, G. E.; Ernzerhof, M. Hybrid Functionals Based on a Screened Coulomb Potential. *J. Chem. Phys.* **2003**, *118*, 8207−8215.
(48) Runge, E.; Gross, E. K. U. Density-Functional Theory for Time-Dependent Systems. *Phys. Rev. Lett.* **1984**, *52*, 997−1000.
(49) Kronik, L.; Neaton, J. B. Excited-State Properties of Molecular Solids from First Principles. *Annu. Rev. Phys. Chem.* **2016**, *67*, 587−616.
(50) Refaely-Abramson, S.; Jain, M.; Sharifzadeh, S.; Neaton, J. B.; Kronik, L. Solid-State Optical Absorption from Optimally Tuned Time-Dependent Range-Separated Hybrid Density Functional Theory. *Phys. Rev. B: Condens. Matter Mater. Phys.* **2015**, *92*, 081204.
(51) Refaely-Abramson, S.; Sharifzadeh, S.; Jain, M.; Baer, R.; Neaton, J. B.; Kronik, L. Gap Renormalization of Molecular Crystals from Density-Functional Theory. *Phys. Rev. B: Condens. Matter Mater. Phys.* **2013**, *88*, 081204.
(52) Gao, Y.; Zhang, M.; Zhang, X.; Lu, G. Decreasing Exciton Binding Energy in Two-Dimensional Halide Perovskites by Lead Vacancies. *J. Phys. Chem. Lett.* **2019**, *10*, 3820−3827.
(53) Huang, L.-y.; Zhang, X.; Zhang, M.; Lu, G. Optically Inactive Defects in Monolayer and Bilayer Phosphorene: A First-Principles Study. *Phys. Rev. Materials* **2018**, *2*, 054003.
(54) Huang, L.-y.; Zhang, X.; Zhang, M.; Lu, G. Effect of Point Defects on Optical Properties of Graphene Fluoride: A First-Principles Study. *J. Phys. Chem. C* **2017**, *121*, 12855−12862.
(55) Frisch, M. J.; Trucks, G. W.; Schlegel, H. B.; Scuseria, G. E.; Robb, M. A.; Cheeseman, J. R.; Scalmani, G.; Barone, V.; Mennucci, B.; Petersson, G. A.; et al. *Gaussian 09*, Revision D.01; Gaussian, Inc.: Wallingford, CT, 2009.
(56) Yuan, M.; Quan, L. N.; Comin, R.; Walters, G.; Sabatini, R.; Voznyy, O.; Hoogland, S.; Zhao, Y.; Beauregard, E. M.; Kanjanaboos, P.; et al. Perovskite Energy Funnels for Efficient Light-Emitting Diodes. *Nat. Nanotechnol.* **2016**, *11*, 872−877.
(57) Tanaka, K.; Sano, F.; Takahashi, T.; Kondo, T.; Ito, R.; Ema, K. Two-Dimensional Wannier Excitons in A Layered-Perovskite-Type Crystal $(C_6H_{13}NH_3)_2PbI_4$. *Solid State Commun.* **2002**, *122*, 249−252.
(58) Jana, M. K.; Liu, C.; Lidin, S.; Dirkes, D. J.; You, W.; Blum, V.; Mitzi, D. B. Resolving Rotational Stacking Disorder and Electronic Level Alignment in a 2D Oligothiophene-Based Lead Iodide Perovskite. *Chem. Mater.* **2019**, *31*, 8523−8532.


https://dx.doi.org/10.1021/acs.jpclett.0c02135
J. Phys. Chem. Lett. 2020, 11, 6982−6989

(59) Liu, Y.; Zhang, Y.; Yang, Z.; Ye, H.; Feng, J.; Xu, Z.; Zhang, X.; Munir, R.; Liu, J.; Zuo, P.; et al. Multi-Inch Single-Crystalline Perovskite Membrane for High-Detectivity Flexible Photosensors. *Nat. Commun.* **2018**, *9*, 5302.
(60) Braun, M.; Tuffentsammer, W.; Wachtel, H.; Wolf, H. C. Tailoring of Energy Levels in Lead Chloride Based Layered Perovskites and Energy Transfer Between the Organic and Inorganic Planes. *Chem. Phys. Lett.* **1999**, *303*, 157−164.
(61) Yu, J.; Kong, J.; Hao, W.; Guo, X.; He, H.; Leow, W. R.; Liu, Z.; Cai, P.; Qian, G.; Li, S.; et al. Broadband Extrinsic Self-Trapped Exciton Emission in Sn-Doped 2D Lead-Halide Perovskites. *Adv. Mater.* **2018**, *31*, 1806385.
(62) Leveillee, J.; Katan, C.; Even, J.; Ghosh, D.; Nie, W.; Mohite, A. D.; Tretiak, S.; Schleife, A.; Neukirch, A. J. Tuning Electronic Structure in Layered Hybrid Perovskites with Organic Spacer Substitution. *Nano Lett.* **2019**, *19*, 8732−8740.
(63) Ema, K.; Inomata, M.; Kato, Y.; Kunugita, H.; Era, M. Nearly Perfect Triplet-Triplet Energy Transfer from Wannier Excitons to Naphthalene in Organic-Inorganic Hybrid Quantum-Well Materials. *Phys. Rev. Lett.* **2008**, *100*, 257401.



https://dx.doi.org/10.1021/acs.jpclett.0c02135
*J. Phys. Chem. Lett.* 2020, 11, 6982−6989